

# Controllable Tunneling of Single Flux Quanta Mediated by Quantum Phase Slip in Disordered Superconducting Loops

J.A. Potter<sup>✉,†</sup>, J.C. Fenton, and P.A. Warburton

*London Centre for Nanotechnology, UCL, 17-19 Gordon Street, London WC1H 0AH, United Kingdom*



(Received 25 March 2022; revised 3 October 2022; accepted 5 January 2023; published 1 February 2023)

Quantum phase slip (QPS) is the exact dual to the well-known Josephson effect. Although there are numerous proposals for applications of QPS devices, experimental work to develop these remains in the relatively early stages. Significant barriers to exploiting QPS nanowires for useful technologies still exist, such as establishing robust nanowire-fabrication methods that allow coupling to low-loss circuits, and demonstrating control over the QPS process with an experimenter-controlled external bias. Here we report experiments that show that both of these barriers have been overcome. We present measurements at 300 mK of NbN coplanar-waveguide (CPW) resonators embedded with nanowires fabricated using a neon focused ion beam. The internal quality factor exceeds  $2 \times 10^4$ —significantly higher than previously reported in comparable experiments. The resonator frequency tunes periodically with an applied magnetic field, revealing tunneling of the order parameter that always occurs at half-integer values of the applied flux. In contrast to previous studies of single QPS, the order-parameter tunneling is shown to be adiabatic, demonstrating improved control over energy dissipation in nanowire QPS circuits. Our results highlight a promising pathway towards realizing low-loss nanowire-based QPS devices.

DOI: 10.1103/PhysRevApplied.19.024002

## I. INTRODUCTION

Quantum circuits based on superconducting materials are currently the leading candidate for the implementation of a scalable quantum computer, already beginning to tackle relevant computation and simulation problems [1,2] and recently demonstrating “quantum advantage” [3]. The Josephson junction is near ubiquitous in these circuits, providing the necessary nonlinearity. A quantum phase-slip nanowire is the flux-charge dual to the Josephson junction [4], and in theory every Josephson-junction-based circuit has a QPS dual. As well as being proposed as a qubit with favorable properties over traditional Josephson-based technology [5,6], the QPS nanowire’s dual property of a nonlinear quantum capacitance enables potential applications such as qubit-qubit couplers [7], parametric amplification for qubit readout, and a primary quantum current standard [8]. As yet, the huge potential of QPS nanowires remains to be fully exploited, and two key reasons for this stand out. Firstly, consistent and reliable fabrication of materials and nanowires with the requisite properties remains challenging; secondly, full control over individual QPS events in a nanowire has not yet been demonstrated.

The QPS phenomenon is most pronounced in quasi-one-dimensional superconducting nanowires, by which we

mean that the cross-sectional dimensions of the nanowire are comparable to the coherence length  $\xi$  [9]. In these nanowires, quantum (or indeed thermal) fluctuations can lead to complete suppression of the superconducting order parameter over the cross section of the wire. This in turn leads to a sudden change of  $2\pi$  in the phase difference between the two ends of the wire, accompanied by the transfer of a quantized amount of magnetic flux equal to the magnetic flux quantum  $\Phi_0 = h/2e$  through the wire. This tunneling of a flux quantum can be coherent [10–12] or incoherent [13], depending on the relative scales of the phase-slip energy  $E_S$  and the inductive energy  $E_L$  of the nanowire. When  $E_S/E_L < 1$ , the magnetic flux quantum number is well defined, and incoherent transfer of individual flux quanta is observable. This is in direct analogy to small Josephson junctions with large charging energy, where tunneling of single Cooper pairs can be observed [14]. It is the incoherent QPS regime that is the focus of this paper. Incoherent QPS occurs probabilistically, with a frequency characterized by the phase-slip rate  $\Gamma_S \equiv E_S/h$ . However, if one waits for a time  $\tau$  that is much longer than  $1/\Gamma_S$ , then flux-quantum tunneling will occur with extremely high likelihood. A device displaying deterministic transfer of quantized amounts of magnetic flux may find useful applications in tasks such as energy-efficient classical digital logic processing [15–19]. Development of such a device is a key enabling technology for control of superconducting quantum processors at technologically useful scales.

\*jamie.potter@npl.co.uk

†Present address: National Physical Laboratory, Teddington, TW11 0LW, United Kingdom.

Historically, phase slips were studied in externally connected, current-biased nanowires, where the collective effect of many phase slips manifests as a resistance below  $T_c$  [20–25]. However, in order to isolate a single phase slip, it is necessary to incorporate the nanowire into a flux-biased superconducting loop. The flux-dependent energy states of a continuous superconducting loop are described by a set of parabolas [see Fig. 1(a)], where each parabola corresponds to a unique value  $N$  of the phase winding number, or equivalently the number of flux quanta in the loop. A single phase slip corresponds to a transition

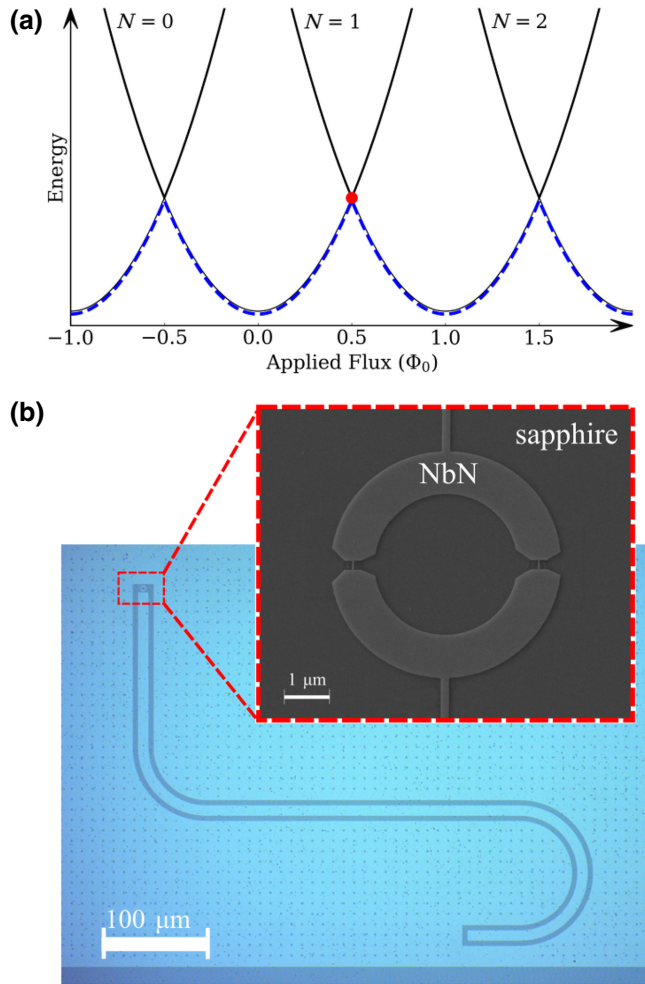


FIG. 1. (a) Flux-dependent energy spectrum of a continuous superconducting loop, with the blue dashed line highlighting the ground state. A single flux quantum may tunnel into the loop at the degeneracy point—highlighted in red.  $N$  is the winding number and  $\Phi_0$  the flux quantum. (b) Optical (main image; blue contrast) and SEM (inset; gray contrast) images of the NbN nanowire-embedded loop located at the short-circuited termination of the CPW resonator. The nanowires in this device are 25 nm wide and 200 nm long. The lower and upper leads to the loop are connected to the CPW center conductor and superconducting ground plane, respectively.

between neighboring parabolas, and if no lower-energy state is available at a particular external flux bias, then phase slips are forbidden. When sweeping the externally applied flux, tunneling of a single flux quantum becomes allowed at  $\Phi_{\text{app}} = (N + 1/2)\Phi_0$  [known as the degeneracy point, highlighted in red in Fig. 1(a)] [26,27]. Tunneling will occur when the system passes the degeneracy point if the rate of phase slips is much greater than the rate at which the flux is swept. However, if the flux is swept quickly with respect to  $\Gamma_S$ , the system will enter a metastable state and it will then undergo irreversible relaxation to the ground state at some later time. A number of recent experiments [28–31] have demonstrated relaxation via QPS from a higher-energy metastable state, but controlled single-flux-quantum tunneling when passing through the degeneracy point has not previously been demonstrated.

In this paper, we demonstrate single-flux-quantum tunneling occurring at the degeneracy point in a continuous superconducting loop. The flux quanta tunnel through NbN nanowires embedded in the loop and this is read out via coupling to a high-quality coplanar waveguide (CPW) resonator. An innovation in our fabrication technique is that the nanowires were fabricated by neon focused-ion-beam (FIB) milling. The FIB process enables the repeatable fabrication of nanowires with width  $w \approx 25$  nm ensuring a large phase-slip rate, while introducing minimal losses to the host resonator. FIB milling has previously been shown to be compatible with low-dissipation superconducting circuits [32,33]; here, we report on the use of FIB to fabricate a device in which quantum phase-slip behavior has been measured. Our results show flux-periodic tuning of the resonant frequency  $\nu_0$  while maintaining a high intrinsic quality factor  $Q_i$  at all values of applied flux. We show that a single quantum phase slip always occurs when adjacent winding-number states become degenerate. This is ensured by a phase-slip rate—we estimate  $\Gamma_S = 35$  MHz—which is large in comparison to  $1/\tau_E$ , where  $\tau_E$  is the experimental timescale. However, the phase-slip rate is less than the inductive energy ( $E_L/h > 1$  THz), and less than the thermal energy ( $k_B T/h \approx 6$  GHz), which excludes the possibility of avoided crossings associated with coherent QPS.

Our demonstration of the ability to control the tunneling of single flux quanta represents progress towards applications of QPS devices in quantum information processing that have been proposed elsewhere. The low loss in our device suggests the potential for high tunneling rates in QPS devices without a significant increase in  $T_1$ -type decoherence. In addition to this, there is potential for a QPS digital logic processing device, based on the deterministic transfer of single flux quanta [15–18]. Utilizing quantum tunneling of flux in such a device should enable significant reduction in the heat dissipation associated with each gate [34], a reduction that will

be necessary for the scaling up of systems beyond the 1000-qubit level.

## II. FABRICATION AND EXPERIMENTAL DETAILS

We fabricate nanowire-embedded resonators from 10-nm-thick films of superconducting NbN. The NbN is deposited on *c*-axis oriented sapphire substrates by dc magnetron sputtering of a 99.99% pure niobium target in a 1:1 Ar:N<sub>2</sub> atmosphere at a pressure of  $5 \times 10^{-3}$  mbar and a power of 150 W. The resulting film is measured to have critical temperature  $T_c = 8.55$  K and sheet resistance  $R_{sq} = 1.2$  k $\Omega$ /sq.

Quarter-wavelength resonators are patterned by electron-beam lithography (EBL) into a 300-nm layer of PMMA resist. Multiple resonators on each chip are capacitively coupled to a common feedline and are patterned with narrow loops galvanically coupled at the short-circuited end. At this stage, the loops contain “precursor” nanowires designed with a width of 400 nm. The pattern is transferred into the NbN film by reactive ion etching (RIE) using a 2:5 volume ratio of CHF<sub>3</sub> and SF<sub>6</sub> at 100 W and 100 mbar.

Nanowires are then patterned into the loops using a neon focused ion beam, whereby a beam of Ne ions is accelerated from an atomically defined tip onto the sample surface with spot size down to 2 nm and sufficient energy to sputter the metal film [35,36]. The precursor wires are milled to a width of 25 nm [see Fig. 1(b)] using a 15-keV Ne beam. A Ne dose of 0.5 nC/ $\mu\text{m}^2$  is sufficient to clear the 10-nm film.

The sample is wire bonded to a copper printed circuit board (PCB) and enclosed within an ECCOSORB-lined brass sample box. This is cooled to a temperature of  $T \sim 300$  mK using a <sup>3</sup>He refrigerator. Measurement of the rf response of the device is made using a vector network analyzer (VNA) via an input line with 60 dB of attenuation to reduce thermal noise from room temperature. Signals in the output line are amplified with a high-electron-mobility-transistor (HEMT) amplifier. Global magnetic field is applied perpendicular to the plane of the loop using a superconducting solenoid and a precision current source. The lines supplying current to the coil are filtered at room temperature with an upper cutoff frequency of 9.2 kHz.

## III. RESULTS AND DISCUSSION

### A. Flux dependence of resonant frequency

In this paper, we present results on a single NbN nanowire-embedded CPW resonator (see Supplemental Material for comparison of multiple devices [37]). We measure the forward transmission ( $S_{21}$ ) through the on-chip feedline, where the  $\lambda/4$  resonators appear as a notch-type resonance. The upper panel of Fig. 2(a) shows the main result of this work: under an applied magnetic field,

the resonance tuning shows discontinuous changes of gradient at periodic values of the applied field. As we demonstrate in the remainder of this paper, these discontinuities occur when two stable states with winding number differing by one become degenerate and are due to single-flux-quantum tunneling mediated by quantum phase slips in the nanowire [38].

The magnetic field periodicity is 153  $\mu\text{T}$ , which corresponds to a single flux quantum in our loop assuming a flux-focusing factor  $\mathcal{F} = 1.7$  [39]. The data in Fig. 2(a) corresponds to a single direction of magnetic field sweep, but sweeps in the opposite direction are found to give the same result. We also observe a nonperiodic, parabolic decrease of the resonant frequency as the magnitude of the applied field is increased. This is the expected [40,41] kinetic inductance tuning of the NbN resonator, and can be parametrized by a phenomenological field-scale  $B_\star = 8$  mT.

Figure 2(a) also shows periodic variation of  $Q_i$  of the resonance as a function of applied field with the same field period as the resonant frequency. Quality factors are obtained by an analytical fit [42] to the equation

$$|S_{21}(\nu)| = ae^{i\alpha} e^{-i2\pi\nu\tau} \left[ 1 - \frac{\left( \frac{Q_l}{|Q_c|} \right) e^{i\phi}}{1 + 2iQ_l(\nu/\nu_0 - 1)} \right], \quad (1)$$

where  $\nu$  is the probe frequency and  $\nu_0$  is the resonance frequency.  $Q_c$  and  $Q_l$  are the coupling and loaded quality factors, respectively, and obey the relationship  $1/Q_l = 1/Q_i + 1/Q_c$ .  $\phi$  accounts for the effect of impedance mismatches in the circuit, the scale factor  $a$  represents the change in amplitude due to any attenuation or amplification in the measurement chain,  $\alpha$  describes any initial phase offset of the signal, and  $\tau$  accounts for frequency-dependent cable delay. We find that  $Q_i$  decreases approximately quadratically from  $4 \times 10^3$  at  $\delta\Phi \equiv (\Phi_{\text{app}} - N\Phi_0)/\Phi_0 = 0$  to  $3.4 \times 10^3$  at  $\delta\Phi = 1/2$ . We attribute this small change to nonequilibrium quasiparticles excited by the induced screening current providing an extra loss mechanism [43]. We observe no sharp decrease in  $Q_i$  at  $\delta\Phi = 1/2$ , which suggests that the heat dissipated by the quantum phase slip itself is not large enough to cause extra losses in the resonator. We note that the intrinsic quality factor exceeds any currently reported in the literature for QPS devices, and discuss this further within the Supplemental Material [37].

The periodic tuning of the resonance is well fitted by a model of an inductive superconducting loop remaining in its ground state [see Fig. 2(b)], where the system is allowed to move between adjacent parabolas by transferring a single flux quantum through the nanowire at  $\Phi_{\text{app}} = (N + 1/2)\Phi_0$ .

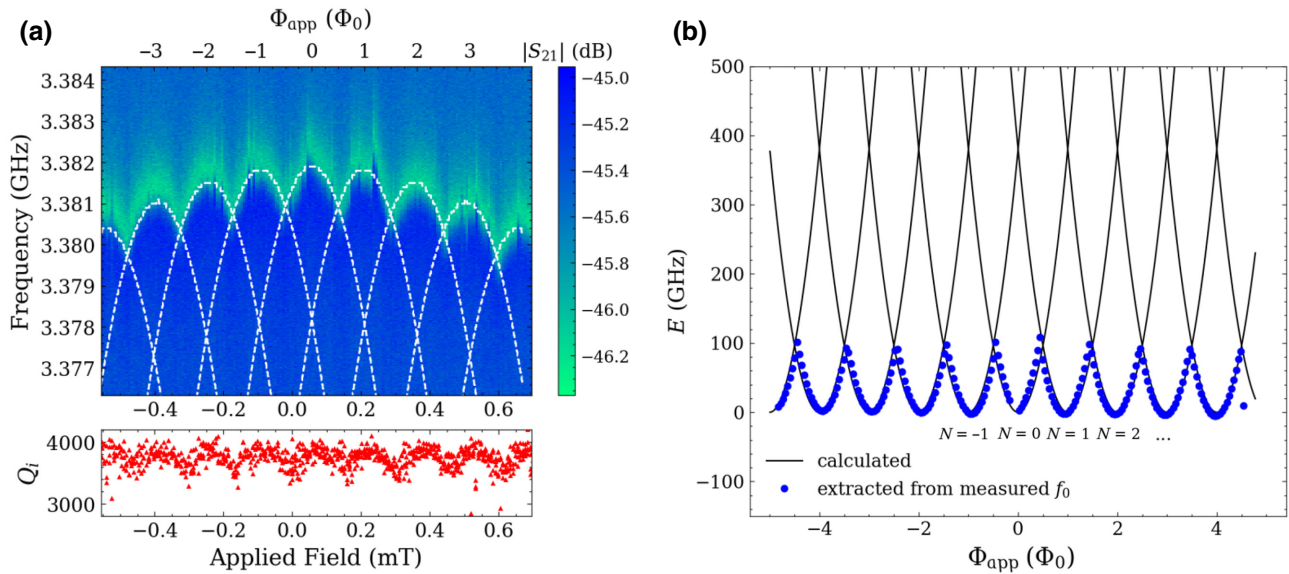


FIG. 2. (a) Upper panel: single-tone spectroscopy of nanowire-embedded resonator measured at  $T = 305$  mK and  $\langle n \rangle \approx 50$ .  $|S_{21}|$  is plotted as a function of frequency and applied magnetic field. The top axis shows the applied magnetic flux  $\Phi_{\text{app}}$  seen by the nanowire loop, which is inferred from the periodicity of the resonator tuning. Dashed white lines show resonant frequencies corresponding to the calculated energy states of the loop. Lower panel: magnetic-field dependence of the measured intrinsic quality factor. (b) Calculated energy states of the loop and values extracted from the measured resonant frequency.

The loop is made up of a wide section and a narrow section [as shown in Fig. 1(b)], and so can be modeled as two nonlinear kinetic inductances in series. The flux-dependent kinetic inductance of the loop  $L_k(\Phi)$  is therefore

$$L_k(I) = L_{k,1}(0) \left[ 1 + \left( \frac{I_s}{I_{*,1}} \right)^2 \right] + L_{k,2}(0) \left[ 1 + \left( \frac{I_s}{I_{*,2}} \right)^2 \right], \quad (2)$$

where  $I_{*,1}$  and  $I_{*,2}$  are known to be of the order of the critical current in the wide and narrow section, respectively [44]. Since the screening current is  $I_s = \Phi/L_k$ , we can insert this into Eq. (2) and solve for  $L_k(\Phi)$ .

The input impedance  $Z_{\text{in}}$  of a  $\lambda/4$  CPW resonator terminated by an inductive load, as a function of frequency and load impedance, is

$$Z_{\text{in}}(\nu, Z_L) = Z_0 \frac{Z_L + iZ_0 \tan\left(\frac{2\pi\nu l}{c}\right)}{Z_0 + iZ_L \tan\left(\frac{2\pi\nu l}{c}\right)}, \quad (3)$$

where  $Z_0$  is the characteristic impedance of the resonator,  $Z_L(\Phi) = i2\pi\nu L_k(\Phi)$  is the impedance of the inductive load,  $c$  is the speed of light in the resonator, and  $l$  is its length. At resonance,  $\text{Im}\{Z_{\text{in}}\} \rightarrow \infty$ , so given  $L_k(\Phi)$  one can numerically calculate  $\nu_0(\Phi)$ , or given  $\nu_0(\Phi)$  one can numerically calculate  $L_k(\Phi)$ .

One can also calculate the flux-dependent free energy of the loop  $E(\Phi)$  from  $L_k(\Phi)$ , using the relation

$$L_k^{-1} = \frac{d^2E}{d\Phi^2}. \quad (4)$$

To obtain the free energy, we simply numerically integrate the inverse of the inductance twice with respect to flux.

We calculate  $L_k(\Phi)$  for our device from Eq. (2) using only independently determined parameters. A critical current density of  $J_c = 4.4 \times 10^5$  Acm $^{-2}$  is obtained from a dc measurement of a track etched into the NbN film, and a sheet kinetic inductance of  $L_{\text{sq}} = 0.34$  nH/sq is inferred from the zero field  $\nu_0$  of the resonator. The geometry of the loop is measured by SEM and this is used to calculate  $L_k(0)$  and  $I_*$  (we set  $I_* = I_c$ ). We then calculate the white dashed lines in Fig. 2(a) using Eq. (3), and the solid black lines in Fig. 2(b) from Eq. (4). The blue points in Fig. 2(b) are extracted from the measured  $\nu_0$  using Eqs. (3) and (4).

## B. Mechanisms for flux quantum transfer

The periodic tuning of the resonator and the associated fit to the calculated energy states of the loop constitute strong evidence that the loop remains in its ground state for all values of  $\Phi_{\text{app}}$ , and this is made possible by a single flux quantum transferring into or out of the loop at  $\delta\Phi = 1/2$ . In order to establish the mechanism by which the flux is able to enter the loop, we now turn our attention to the transitions between flux states. Across multiple devices on multiple chips, we find an onset of flux-periodic

tuning in devices containing nanowires with  $w \lesssim 35$  nm. This dependence of the behavior on nanowire width suggests that the flux tunneling occurs in the nanowires, and not in the wider part of the loop. We can now examine some possible physical processes that could occur in the nanowires and see how the data fits with them.

*-Does the nanowire current exceed its critical current  $I_c^{\text{nw}}$ ?* Niobium-nitride resonators commonly exhibit a nonlinear  $S_{21}$  response when they are driven with a high microwave power [45] as a result of the current-induced nonlinear kinetic inductance. As we see in Eq. (2), the kinetic inductance is quadratically dependent on  $(I/I_c)^2$ , and so the nonlinearity must be dominated by the part of the conductor with the lowest  $I_c$ . This is confirmed by measurements of our circuits, where we find that nanowire-embedded resonators show a much higher degree of nonlinearity in their  $S_{21}$  response than bare resonators (see the Supplemental Material [37]). The quadratic nature of the nonlinearity suggests that a strongly nonlinear response is a consequence of the magnitude of the rf current  $I_{\text{res}}$  in the resonator reaching a significant fraction of the nanowire critical current  $I_c^{\text{nw}}$ . Our NbN resonator readout method therefore gives us an indirect readout of whether the current in the nanowire is close to  $I_c^{\text{nw}}$ .

Figure 3 shows the  $S_{21}$  response of the nanowire-embedded resonator at  $\delta\Phi = 0$  and  $\delta\Phi = 1/2$ , both measured in the low-power limit with an estimated resonator photon population of  $\langle n \rangle \approx 50$ . In both cases, the response is linear and well fitted by Eq. (1). We calculate, using the relation  $I_s = dE(\Phi)/d\Phi$  that the maximum induced screening current in the nanowires  $I_s(\delta\Phi = 1/2)$  is 120 nA, an order of magnitude less than  $I_c^{\text{nw}}$ . Crucially, the lack of nonlinearity of the resonance at  $\delta\Phi = 1/2$ , along with the fact that  $Q_i$  remains a significant fraction of its zero-field value, means that the nanowires are not being driven close to their critical current by the applied flux. By a similar argument, we know that the nanowires are not being driven through  $T_c$  by a local heating process, as this would also result in nonlinearity of the resonance at  $\delta\Phi = 1/2$  due to dissipation in the highly resistive normal metal.

*-Is the nanowire a constriction Josephson junction?* “Dayem-bridge” Josephson-junction superconducting quantum interference devices (SQUIDs) are commonly embedded within CPW resonators [46,47] to provide a flux-tunable resonant frequency. However, when the SQUID loop has a large inductance, one observes hysteretic tuning, characterized by the parameter  $\beta_L = 2LI_c/\Phi_0$ . When  $\beta_L \gtrsim 1$ , the SQUID behavior becomes hysteretic with applied flux and the resonator will exhibit discontinuous jumps in the resonant frequency, as observed in Refs. [48,49]. Our device does not undergo any discontinuous jumps, and the tuning over a single flux quantum is symmetric, so  $\beta_L < 1$ . Given this and the known loop inductance, we can set an upper bound on the critical current of any Josephson junction of  $I_c^{\text{JJ}} < 100$  nA.

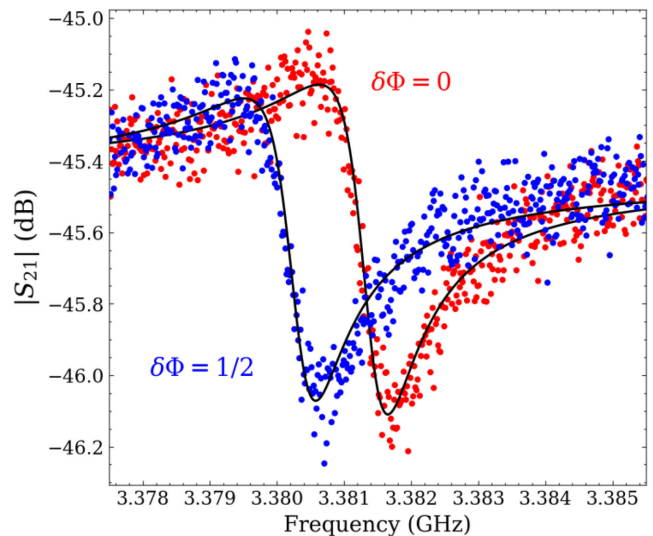


FIG. 3.  $|S_{21}|$  measured at  $\Phi_{\text{app}} = 0$  and  $\Phi_{\text{app}} = \Phi_0/2$  along with fit (black line) to a linear resonance model. This shows that at  $\Phi_{\text{app}} = \Phi_0/2$  the response is linear, so the current in the nanowire is well below the critical current.

This bound is  $10\times$  smaller than the expected transport critical current of our nanowires and also less than  $I_s(\delta\Phi_0)$ . Therefore, it is unrealistic to conclude that the flux tuning we observe is a consequence of a dc SQUID formed of Dayem-bridge Josephson junctions. We also note that the closeness of the fit shown in Fig. 2 suggests there is no contribution to the flux-dependent inductance from a Josephson junction, which would add a  $1/\cos\Phi$  term to Eq. (2).

*-Is this a thermal or quantum process?* Figure 4 shows that tunneling always occurs at degeneracy. Following Petković *et al.* [30],  $\Delta\phi_N^+$  is defined as  $\Delta\phi_N^+ = \phi_N^+ - \phi_{\min,N}$ , where  $\phi_N^+$  is the normalized flux  $\phi = \Phi/\Phi_0$  at which tunneling from state  $N$  to state  $N + 1$  occurs, and  $\phi_{\min,N}$  is the flux that minimizes the loop free energy for a particular winding number  $N$ . Our data shows the periodicity, defined in this way, to be half a flux quantum for all values of the winding number except  $N = 1$  (we attribute the latter exception to enhanced flux focusing at low magnetic field). This is in contrast to Ref. [30], where a characteristic dependence of  $\Delta\phi_N^+$  on  $N$  is shown to be a defining feature of thermally activated phase slips. By following the method of Ref. [30], we calculate that  $\Delta\phi_N^+ \approx 300$  would be required in order for the energy barrier to phase slips in our nanowire to be tuned to  $\lesssim k_B T$ . Correspondingly, we can estimate (see the Supplemental Material [37,50–53]) that  $\Gamma_{\text{QPS}} = 35$  MHz for our nanowire, and we calculate a temperature-dependent  $\Gamma_{\text{TAPS}}$  that is below 1 Hz for  $T < 1.5$  K. Therefore, at our measurement temperature, quantum tunneling of flux is overwhelmingly more likely than a thermal transition. For comparison, the inverse experimental timescale is

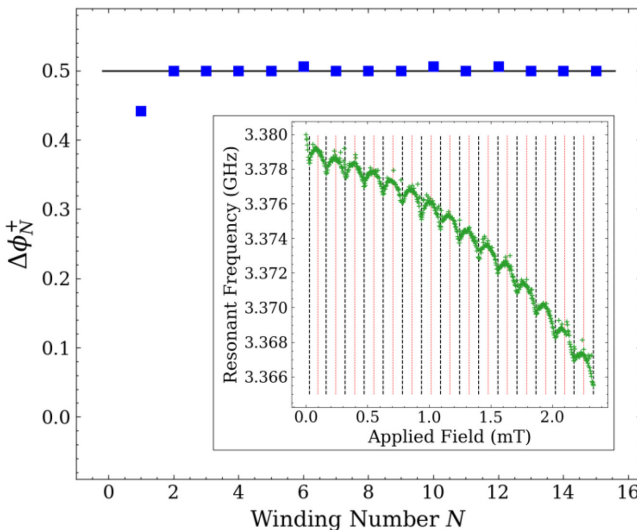


FIG. 4. Normalized tunneling flux  $\Delta\phi_N^+$  (defined in the main text), as a function of the winding number  $N$ . The solid line corresponds to half a flux quantum,  $\Delta\phi_N^+ = 0.5$ . Inset: magnetic-field dependence of resonant frequency of the nanowire-embedded resonator up to an applied field of 2.4 mT. The black dotted lines mark transitions between winding number states ( $\phi_N^+$ ), and the red dotted lines mark the energy minimum of each winding number state ( $\phi_{\min,N}$ ).

$1/\tau_E \approx 0.2$  Hz since, for each setpoint of the magnetic field, it takes the VNA approximately 5 s to collect  $S_{21}$  data across the resonance. Because, in contrast to previous studies,  $k_B T/h > \Gamma_{\text{QPS}} \gg 1/\tau_E$  when our device bias is swept through the degeneracy point, a single quantum phase slip always occurs before we are able to observe the system in a higher-energy metastable state.

#### IV. CONCLUSIONS

We use a Ne FIB to fabricate NbN nanowires with widths down to 25 nm embedded within CPW resonators. We observe periodic modulation of resonant frequency and intrinsic quality factor, which is consistent with quantum tunneling of individual flux quanta mediated by quantum phase slip, occurring when states of different winding number become degenerate. This behavior has been observed in resonators with intrinsic quality factor,  $Q_i$ , up to  $2.7 \times 10^4$  at 300 mK, and we note that the losses here are significantly lower than reported in comparable studies [10]. We estimate that the QPS rate is of the order 10–100 MHz, which means that the tunneling of a single flux quantum is effectively deterministic on the timescale of microseconds. This result shows the suitability of the Ne FIB process for fabricating QPS devices. We also suggest that an incoherent QPS device with a high QPS rate such as ours could be promising for classical digital logic processing applications, where the quantum nature of the flux tunneling implies a reduction in heat dissipation compared

with current state-of-the-art devices, opening up a route to resolving a roadblock to the upscaling of qubit control electronics.

#### ACKNOWLEDGMENTS

The authors thank O.W. Kennedy for useful discussions. The authors gratefully acknowledge funding from the United Kingdom Engineering and Physical Sciences Research Council, Grants No. EP/L015242/1, No. EP/J017329/1, and No. EP/T001062/1.

- [1] F. Arute, *et al.*, Hartree-Fock on a superconducting qubit quantum computer, *Science* **369**, 1084 (2020).
- [2] S. Yarkoni, F. Neukart, E. M. G. Tagle, N. Magiera, B. Mehta, K. Hire, S. Narkhede, and M. Hofmann, in *Proceedings of the 1st ACM SIGSOFT International Workshop on Architectures and Paradigms for Engineering Quantum Software*, APEQS 2020 (2020), p. 22.
- [3] F. Arute, *et al.*, Quantum supremacy using a programmable superconducting processor, *Nature (London)* **574**, 505 (2019).
- [4] J. E. Mooij and Y. V. Nazarov, Superconducting nanowires as quantum phase-slip junctions, *Nat. Phys.* **2**, 169 (2006).
- [5] J. E. Mooij and C. J. P. M. Harmans, Phase-slip flux qubits, *New J. Phys.* **7**, 219 (2005).
- [6] D. T. Le, A. Grimsmo, C. Müller, and T. M. Stace, Doubly nonlinear superconducting qubit, *Phys. Rev. A* **100**, 062321 (2019).
- [7] A. J. Kerman, Superconducting qubit circuit emulation of a vector spin-1/2, *New J. Phys.* **21**, 073030 (2019).
- [8] Z. M. Wang, J. S. Lehtinen, and K. Y. Arutyunov, Towards quantum phase slip based standard of electric current, *Appl. Phys. Lett.* **114**, 242601 (2019).
- [9] A. Bezryadin, Quantum suppression of superconductivity in nanowires, *J. Phys. Condens. Matter* **20**, 043202 (2008).
- [10] O. Astafiev, L. Ioffe, S. Kafanov, Y. A. Pashkin, K. Y. Arutyunov, D. Shahar, O. Cohen, and J. Tsai, Coherent quantum phase slip, *Nature (London)* **484**, 355 (2012).
- [11] J. Peltonen, O. Astafiev, Y. P. Korneeva, B. Voronov, A. Korneev, I. Charaev, A. Semenov, G. Golt'sman, L. Ioffe, and T. Klapwijk, *et al.*, Coherent flux tunneling through NbN nanowires, *Phys. Rev. B* **88**, 220506 (2013).
- [12] J. Peltonen, Z. Peng, Y. P. Korneeva, B. Voronov, A. Korneev, A. Semenov, G. Golt'sman, J. Tsai, and O. Astafiev, Coherent dynamics and decoherence in a superconducting weak link, *Phys. Rev. B* **94**, 180508 (2016).
- [13] N. G. N. Constantino, M. S. Anwar, O. W. Kennedy, M. Dang, P. A. Warburton, and J. C. Fenton, Emergence of quantum phase-slip behaviour in superconducting NbN nanowires: DC electrical transport and fabrication technologies, *Nanomaterials (Basel)* **8**, 442 (2018).

- [14] L. J. Geerligs, V. F. Anderegg, J. Romijn, and J. E. Mooij, Single Cooper-Pair Tunneling in Small-Capacitance Junctions, *Phys. Rev. Lett.* **65**, 377 (1990).
- [15] K. K. Likharev and V. K. Semenov, RSFQ logic/memory family: a new Josephson-junction technology for sub-terahertz-clock-frequency digital systems, *IEEE Trans. Appl. Supercond.* **1**, 3 (1991).
- [16] O. A. Mukhanov, Energy-efficient single flux quantum technology, *IEEE Trans. Appl. Supercond.* **21**, 760 (2011).
- [17] Q. P. Herr, A. Y. Herr, O. T. Oberg, and A. G. Ioannidis, Ultra-low-power superconductor logic, *J. Appl. Phys.* **109**, 103903 (2011).
- [18] D. E. Kirichenko, S. Sarwana, and A. F. Kirichenko, Zero static power dissipation biasing of RSFQ circuits, *IEEE Trans. Appl. Supercond.* **21**, 776 (2011).
- [19] M. H. Volkmann, A. Sahu, C. J. Fourie, and O. A. Mukhanov, Implementation of energy efficient single flux quantum digital circuits with sub-aJ/bit operation, *Supercond. Sci. Tech.* **26**, 015002 (2012).
- [20] J. Lukens, R. Warburton, and W. Webb, Onset of Quantized Thermal Fluctuations in “One-Dimensional” Superconductors, *Phys. Rev. Lett.* **25**, 1180 (1970).
- [21] R. Newbower, M. Beasley, and M. Tinkham, Fluctuation effects on the superconducting transition of tin whisker crystals, *Phys. Rev. B* **5**, 864 (1972).
- [22] A. Van Run, J. Romijn, and J. Mooij, Superconduction phase coherence in very weak aluminium strips, *Jpn. J. Appl. Phys.* **26**, 1765 (1987).
- [23] N. Giordano, Evidence for Macroscopic Quantum Tunneling in One-Dimensional Superconductors, *Phys. Rev. Lett.* **61**, 2137 (1988).
- [24] A. Bezryadin, C. N. Lau, and M. Tinkham, Quantum suppression of superconductivity in ultrathin nanowires, *Nature (London)* **404**, 971 (2000).
- [25] C. N. Lau, N. Markovic, M. Bockrath, A. Bezryadin, and M. Tinkham, Quantum Phase Slips in Superconducting Nanowires, *Phys. Rev. Lett.* **87**, 217003 (2001).
- [26] K. A. Matveev, A. I. Larkin, and L. I. Glazman, Persistent Current in Superconducting Nanorings, *Phys. Rev. Lett.* **89**, 096802 (2002).
- [27] X. Zhang and J. C. Price, Susceptibility of a mesoscopic superconducting ring, *Phys. Rev. B* **55**, 3128 (1997).
- [28] A. Belkin, M. Brenner, T. Aref, J. Ku, and A. Bezryadin, Little–Parks oscillations at low temperatures: Gigahertz resonator method, *Appl. Phys. Lett.* **98**, 242504 (2011).
- [29] A. Belkin, M. Belkin, V. Vakaryuk, S. Khlebnikov, and A. Bezryadin, Formation of Quantum Phase Slip Pairs in Superconducting Nanowires, *Phys. Rev. X* **5**, 021023 (2015).
- [30] I. Petković, A. Lollo, L. Glazman, and J. Harris, Deterministic phase slips in mesoscopic superconducting rings, *Nat. Commun.* **7**, 13551 (2016).
- [31] I. Petkovic, A. Lollo, and J. G. E. Harris, Phase-Slip Statistics of a Single Isolated Flux-Biased Superconducting Ring, *Phys. Rev. Lett.* **125**, 067002 (2020).
- [32] J. Burnett, J. Sagar, P. Warburton, and J. Fenton, Embedding NbN nanowires into quantum circuits with a neon focused ion beam, *IEEE Trans. Appl. Supercond.* **26**, 1 (2016).
- [33] J. Burnett, J. Sagar, O. W. Kennedy, P. A. Warburton, and J. C. Fenton, Low-Loss Superconducting Nanowire Circuits using a Neon Focused Ion Beam, *Phys. Rev. Appl.* **8**, 014039 (2017).
- [34] R. McDermott, M. G. Vavilov, B. L. T. Plourde, F. K. Wilhelm, P. J. Liebermann, O. A. Mukhanov, and T. A. Ohki, Quantum–classical interface based on single flux quantum digital logic, *Quantum Sci. Technol.* **3**, 024004 (2018).
- [35] D. Petit, C. C. Faulkner, S. Johnstone, D. Wood, and R. P. Cowburn, Nanometer scale patterning using focused ion beam milling, *Rev. Sci. Instr.* **76**, 026105 (2005).
- [36] H. Wu, D. Ferranti, and L. Stern, Precise nanofabrication with multiple ion beams for advanced circuit edit, *Microelectron. Reliab.* **54**, 1779 (2014).
- [37] See Supplemental Material at <http://link.aps.org/supplemental/10.1103/PhysRevApplied.19.024002> for data showing reproducibility of multiple devices, comparison of resonator quality factors, a demonstration of kinetic inductance nonlinearity, and calculations of phase-slip rates.
- [38] K. Y. Arutyunov, D. S. Golubev, and A. D. Zaikin, Superconductivity in one dimension, *Phys. Rep.* **464**, 1 (2008).
- [39] D. Bothner, D. Wiedmaier, B. Ferdinand, R. Kleiner, and D. Koelle, Improving Superconducting Resonators in Magnetic Fields by Reduced Field Focussing and Engineered Flux Screening, *Phys. Rev. Appl.* **8**, 034025 (2017).
- [40] J. E. Healey, T. Lindström, M. S. Colclough, C. M. Muirhead, and A. Y. Tzalenchuk, Magnetic field tuning of coplanar waveguide resonators, *Appl. Phys. Lett.* **93**, 043513 (2008).
- [41] C. W. Zollitsch, J. O’Sullivan, O. Kennedy, G. Dold, and J. J. L. Morton, Tuning high-Q superconducting resonators by magnetic field reorientation, *AIP Adv.* **9**, 125225 (2019).
- [42] S. Probst, F. Song, P. Bushev, A. Ustinov, and M. Weides, Efficient and robust analysis of complex scattering data under noise in microwave resonators, *Rev. Sci. Instr.* **86**, 024706 (2015).
- [43] J. L. Levine, Dependence of Superconducting Energy Gap on Transport Current by the Method of Electron Tunneling, *Phys. Rev. Lett.* **15**, 154 (1965).
- [44] J. Zmuidzinas, Superconducting microresonators: Physics and applications, *Annu. Rev. Condens. Matter Phys.* **3**, 169 (2012).
- [45] C. N. Thomas, S. Withington, Z. Sun, T. Skyrme, and D. J. Goldie, Nonlinear effects in superconducting thin film microwave resonators, *New J. Phys.* **22**, 073028 (2020).
- [46] A. Palacios-Laloy, F. Nguyen, F. Mallet, P. Bertet, D. Vion, and D. Esteve, Tunable resonators for quantum circuits, *J. Low Temp. Phys.* **151**, 1034 (2008).
- [47] M. Sandberg, C. M. Wilson, F. Persson, T. Bauch, G. Johansson, V. Shumeiko, T. Duty, and P. Delsing, Tuning the field in a microwave resonator faster than the photon lifetime, *Appl. Phys. Lett.* **92**, 203501 (2008).
- [48] E. M. Levenson-Falk, R. Vijay, and I. Siddiqi, Nonlinear microwave response of aluminum weak-link Josephson oscillators, *Appl. Phys. Lett.* **98**, 123115 (2011).

- [49] O. Kennedy, J. Burnett, J. Fenton, N. Constantino, P. Warburton, J. Morton, and E. Dupont-Ferrier, Tunable Nb Superconducting Resonator Based on a Constriction Nano-SQUID Fabricated with a Ne Focused Ion Beam, *Phys. Rev. Appl.* **11**, 014006 (2019).
- [50] J. Mooij, G. Schön, A. Shnirman, T. Fuse, C. Harmans, H. Rotzinger, and A. Verbruggen, Superconductor–insulator transition in nanowires and nanowire arrays, *New J. Phys.* **17**, 033006 (2015).
- [51] J. S. Langer and V. Ambegaokar, Intrinsic resistive transition in narrow superconducting channels, *Phys. Rev.* **164**, 498 (1967).
- [52] D. E. McCumber and B. I. Halperin, Time scale of intrinsic resistive fluctuations in thin superconducting wires, *Phys. Rev. B* **1**, 1054 (1970).
- [53] M. Tinkham and C. N. Lau, Quantum limit to phase coherence in thin superconducting wires, *Appl. Phys. Lett.* **80**, 2946 (2002).